Cost-Optimal Hydrogen Refueling Scheduling for Bus Fleet in a Grid-Connected Hybrid Renewable Energy System

Sarad Basnet[a,*], Karine Deschinkel[a], Luis Le Moyne[b] and Marie Cécile Péra[a]

[a]Université Marie & Louis Pasteur, FEMTO-ST, FCLAB, CNRS, 90000, Belfort, France
[b]Université de Bourgogne, ISAT, DRIVE, 58000, Nevers, France

ARTICLE INFO

Keywords:
Hydrogen mobility
Hybrid renewable energy system
Refueling scheduling
MILP co-optimization
Levelized cost of hydrogen
Urban energy systems

Abstract

This study presents a cost-optimal sizing and energy management approach for a grid-integrated hybrid renewable energy system—comprising solar PV, wind turbines, and hydrogen production via electrolyzers with compressed storage—to meet both the electricity demand of Dijon, France, and hydrogen demand for mobility. To better plan the refueling of the hydrogen bus fleet, two case scenarios are analyzed: (i) refueling is flexibly scheduled over 24 hours and (ii) refueling is optimally scheduled but restricted to 3h–7h, both for cost optimization. A Mixed-Integer Linear Programming (MILP) model is formulated and resolved in the developed tool KLMS-OPT using the Pyomo modeling interface in Python with the objective of minimizing total annual cost. In the flexible scenario compared to the restricted scenario, the optimal configuration reduces the number of electrolyzers and refueling points from three to one. The hydrogen storage capacity remains below 100 kg, avoiding the need for legal authorization required in France for larger installations. This configuration yields a 0.35% reduction in annual cost. Ultimately, the formulated problem in KLMS-OPT demonstrates strong computational efficiency, solving all scenarios in less than 20 minutes.

1. Introduction

Alongside the heat and electricity sectors, transportation remains a major contributor to global greenhouse gas (GHG) emissions [1]. The growing population and rising mobility demands, particularly in urban areas, underscore the urgent need for sustainable alternatives. The transition toward low-carbon transport can be viewed from two perspectives: first, as a change in mobility behavior, where communities adopt reduced travel, increased use of public transportation, and car-sharing; and second, as an energy transition within the transport sector, shifting from fossil fuels to renewable energy sources. Battery electric vehicles (BEVs), fuel cell electric vehicles (FCEVs), and hybrid vehicles (HVs) are among the key technologies being adopted [2]. Among these, hydrogen-powered FCEVs represent one of the most promising options. Although the technology has gained attention, the development of hydrogen refueling stations (HRSs) and supporting gas networks remains in its early stages [3], raising critical questions about achieving a cost-effective transition to decarbonized hydrogen mobility in urban areas.

To effectively mitigate GHG emissions, priority should be given to producing green or low-carbon hydrogen (H_2) via electrolysis powered by renewable energy sources. As the adoption of FCEVs expands, the resulting increase in H_2 demand will require additional onsite production and distribution infrastructure, including HRSs. A typical HRS comprises several components, including storage tanks, compressors, and dispensers [4]. Compressors increase the pressure of H_2 gas to 350–1000 bar, depending on storage and dispensing requirements [5], while pre-cooling systems enable safe and efficient high-pressure dispensing. The deployment of refueling stations also requires selecting optimal locations that maximize vehicle coverage while remaining economically viable [6]. As of 2020, approximately 550 HRSs were operational worldwide: 50% in Asia, 33.36% in Europe, and 13.63% in the United States, supporting around 34,800 FCEVs [7]. By 2024, China, South Korea, Japan, France, and Germany each had over 100 active stations, collectively representing 79% of the global total [8]. Integrating the hydrogen ecosystem—including production, storage, and distribution—into hybrid renewable energy systems (HRES) has become increasingly important [9],

*Corresponding author
sarad.basnet@univ-fcomte.fr (S. Basnet)
https://www.linkedin.com/in/saradbasnet/ (S. Basnet)
ORCID(s): 0000-0003-3071-7064 (S. Basnet)

[10]. Typically, these systems optimize economic and environmental performance, offering crucial guidance for the development of sustainable H_2 infrastructure that aligns with decarbonization goals.

While numerous studies have investigated the sizing and operational management of HRES for onsite H_2 production and distribution, few link these aspects with downstream H_2 dispensing at refueling stations [11], [12]. [12] developed a predictive operation strategy for onsite H_2 production at HRS, focusing on intelligent electrolysis scheduling. The strategy leveraged periods of low electricity prices and wind energy integration through participation in the spot market alongside a wind farm. Using real H_2 demand data over a one-week period (168 kg), the study demonstrated reduced H_2 production costs but did not address system sizing or flexible demand management. [13] developed a fully islanded green H_2 system integrating solar photovoltaic (PV), wind turbines (WT), electrolyzers (Elz), batteries, and H_2 storage, designed to meet a constant hourly demand of 10 kg/h. The system achieved a levelized cost of H_2 (LCOH) of €2.89/kg H_2, suitable for isolated communities in the Czech Republic. However, dynamic rescheduling of H_2 demand was not considered. Similarly, [14] performed a techno-economic analysis of onsite PV-WT hybrid systems for H_2 production in Turkey and Spain, determining optimal configurations for daily H_2 demands of 120 kg for 24 FCEVs. LCOH values were 6.15 \$/kg H_2 in Niğde and 5.83 \$/kg H_2 in Zaragoza. Although system sizing and sensitivity analyses were included, optimal dispatching to minimize costs was not addressed.

A dynamic analysis of a self-sustaining HRS powered by renewables was conducted by [15], who measured real-time H_2 demand at a public station in Irvine, California. LCOH could be reduced to 6.71 \$/kg H_2 using either 200 kW of WT or 360 kW of solar PV; however, cost-optimal rescheduling of H_2 production was not investigated. Similarly, [16] examined a decentralized H_2 system in Halle, Belgium, powered by 1.5 MW WT and 1 MW PV. Results suggested that reducing capital costs by 80% could lower LCOH to €6.70/kg H_2, but system sizing and demand optimization were not considered. [17] performed a comprehensive evaluation of hybrid solar PV and WT systems, optimizing the configuration to minimize costs. Their methodology employed a Monte Carlo simulation to model the H_2 refueling demand profile. The results revealed an annual production of 40,000 kg of green H_2, supported by an optimized storage capacity of 600 kg in the H_2 tanks. [3] focused on profitability of onsite HRS production from wind energy, providing insights into H_2 dispensed per refueling event but not on scheduling or dispatch optimization.

Although extensive research has been conducted on the sizing and operation of energy systems, few studies focus on developing or scheduling optimized H_2 dispatch strategies tailored to urban mobility. Such strategies must balance renewable energy availability, electrolyzer operation, tank capacity, and cost-effectiveness. Optimizing these factors ensures efficient H_2 production aligned with bus fleet demand, identifying cost-minimizing refueling hours and maximizing renewable energy utilization. This area represents a key opportunity for research, particularly integrating renewable generation, electrolyzer performance, and storage capacity with refueling profiles reflecting actual fleet behavior. Past research generally addressed H_2 demand with three main formulations: behavior-based, decision variable-based, and target-based, as summarized in Table 1. Behavior-based models studied by [18], [19], and [20] simulated user or vehicle refueling behavior to predict demand from FCEV travel behavior or probabilistic trip data. Decision variable–based models as presented in [6] and [21] incorporate H_2 demand directly into optimization models as an endogenous variable influencing supply and capacity. Target-based studies according to [22], [23], and [24], used prespecified or estimated H_2 demand – typically derived from forecast FCEV deployment – as a prespecified input for network planning or capacity determination. At the strategic and design levels, these studies optimize network topology, installation placement, and storage capacity [19], [21], [22], and [23] under static or aggregate demand. More recent operational-level research studies consider H_2 dispatch and scheduling approaches that dynamically adapt production and storage based on electricity price uncertainty and short-term demand. For example, [20] developed a time-of-use electrolysis scheduling model for electric and H_2 buses, whereas [6] and [21] optimized the flows of H_2 under conditions of uncertain demand. These articles, however, focus primarily on energy management at a single station and not on coordinating refueling operations across a fleet of vehicles.

Recent studies have further explored the operation of HRS in connection with HRES and mobility demand coordination. For instance, two recent works [25], [26] analyze integrated renewable–H_2 configurations in which electrolyzer operation and refueling activities are coordinated to reduce energy cost and environmental impact. While these contributions provide valuable insights into station operation and energy management, they typically assume a fixed hourly H_2 demand profile or a fixed refueling time window. In contrast, the present study proposes a city-scale Mixed

Integer Linear Programming (MILP) framework in which the *hourly refueling pattern* and the *number of active dispensers* are decision variables co-optimized together with PV, wind, and electrolyzer capacities, thereby linking infrastructure sizing with hourly refueling operations in a unified framework.

Literatures	Behavior Based	Decision Var. Based	Target Based	Network / Location Based	Transport	H_2 Demand Model
[6]	✗	✓	✗	✓	Buses & Trucks	Demand estimated from freight and bus data; satisfaction treated as a decision variable.
[19]	✓	✗	✗	✓	Passenger FCEV	Demand estimated from FCEV trip distributions and probabilistic surveys.
[20]	✓	✓	✗	✗	H_2 and electric buses	Demand predicted from user travel data; used as a scheduling decision variable.
[21]	✗	✓	✗	✓	FCEV	Demand treated as an uncertain decision parameter in a two-stage stochastic model.
[22]	✗	✗	✓	✓	FCEV	Forecast-based demand (2020–2022 data); robust model ensures ≥95% satisfaction.
[23]	✗	✗	✓	✗	Heavy-duty trucks	Forecast from operational data (40 trucks/day); demand defined as $H_{load}(d+1)$.
[24]	✗	✗	✓	✗	Not specified	Demand implicitly satisfied through integrated renewable–storage optimization.
This study	✗	✓	✗	✗	H_2 buses	30 buses (414 kg H_2/day); multi-year hourly operation and simulation; cost optimization.

Table 1: Comparison of H_2 Demand Modeling in Recent Studies

The research contribution, summarized alongside existing literature in Table 2, specifically determines the optimal number of buses to refuel each hour and the efficient utilization of refueling points. The model integrates a H_2-based HRES comprising solar PV, wind turbines, the power grid, electrolyzers, and H_2 storage tanks, and couples two energy sectors: city-wide electricity and H_2 demand for mobility. The analysis evaluates multiple technical, economic, and environmental indicators while excluding the sale of excess renewable electricity back to the grid to focus on local utilization.

The paper is structured as follows: section 2 outlines the methodology and problem statement, including a detailed description of the case study location, the optimization framework, and the mathematical formulation used for scheduling. The performance indicators employed to analyze the simulation results are presented in subsection 2.5. The results and corresponding discussions are provided in section 3. Finally, the key conclusions of the study are summarized in section 4.

1.1. Novelty of the study

The present study proposes an integrated modeling and optimization framework for a grid-connected HRES dedicated to H_2 mobility at the city scale. The system combines PV, WT, and grid electricity to supply a HRS serving a fleet of fuel-cell buses. The framework simultaneously addresses system sizing and operational scheduling in a unified formulation.

Unlike previous studies that treat the H_2 demand or the refueling profile as fixed inputs, the hourly refueling pattern and the number of active dispensers are here introduced as decision variables of the optimization problem. This choice enables a realistic coupling between the station's service capacity, the temporal distribution of bus refueling, and the sizing of generation and storage assets.

Level	Highlights	Objectives	Literatures
Strategic	Network layout, siting, sizing, and capacity design	City- or multi-site level planning; long-term demand forecasting	[19], [21], [22], [27], [28]
Design	Optimizing station capacity, sizing storage, and integrating components	Techno-economic optimization with renewable integration	[23], [24]
Energy Management	Operation of integrated charging stations combining electric and H_2 systems	Scheduling and dispatch optimization for hybrid ICS	[20]
Operational–Refueling (Existing Studies)	Station-level refueling optimization; stochastic or predictive modeling	Modeling of refueling patterns or arrival-based demand; single-station focus; no fleet-level scheduling or cost optimization	[25], [26]
Operational–Refueling (This Study)	Fleet-level, hourly optimization of H_2 refueling schedules, dispenser utilization, and on-site H_2 production	Cost minimization and operational scheduling for a bus fleet	**This Study (2025)**

Table 2: Comparison of H_2 Refueling Studies Across Levels

The model integrates service-time and dispenser-throughout constraints, ensuring that the hourly number of refueled buses remains feasible with respect to the available equipment and average refueling duration. It also accounts for electrolyzer operating limits, H_2 storage bounds, and a power-balance equation that couples renewable and grid electricity with H_2 production, providing an accurate representation of the system's operation.

The optimization is formulated as a Mixed-Integer Linear Programming (MILP) problem that remains computationally tractable for city-scale scenarios. The solution provides actionable design and operational insights—such as the required number of dispensers, electrolyzers, and storage capacity—under both flexible and restricted refueling policies.

Finally, the study quantifies how refueling flexibility influences the overall techno-economic performance of the HRES, including the total annual cost (TAC), the levelized cost of H_2 (LCOH), and component utilization. This analysis highlights that strategic coordination between refueling schedules and renewable energy availability can substantially reduce infrastructure needs while maintaining reliable service for the bus fleet.

Overall, the main novelty of this work lies in the joint optimization of system sizing and hourly refueling scheduling, under realistic service and operational constraints, within a comprehensive city-scale MILP framework.

While the present framework adopts a deterministic hourly demand profile, this assumption reflects the lack of available high-resolution stochastic data for bus operations in the Dijon case study. It ensures a transparent and reproducible comparison between refueling policies without compromising generality. The model structure remains readily extensible to stochastic or predictive formulations as finer temporal demand data become available [29], [30].

2. Problem statement and Methodology

Figure 1 presents a urban energy system composed of two interconnected sectors aimed at meeting both electricity and H_2 demands. The city of Dijon, France, is selected as a representative European case study due to its average geographic and demographic features, along with the availability of relevant data on energy consumption and planned H_2-based public transportation. A "Power-to-H_2" subsystem is incorporated within the broader energy network, which addresses electricity needs through a hybrid approach that combines renewable energy sources with grid-supplied power. Key attributes of Dijon—its latitude (47.317), longitude (5.017), time zone (UTC+1), population (261,901), area (40.41 km²), and number of households (155,834)—offer a valuable reference for urban energy modeling in a European context. The system utilizes renewable technologies, specifically solar PV and WT, to supply electricity for both general consumption and H_2 production via electrolyzers, thereby supporting continuous operation of the H_2 refueling infrastructure.

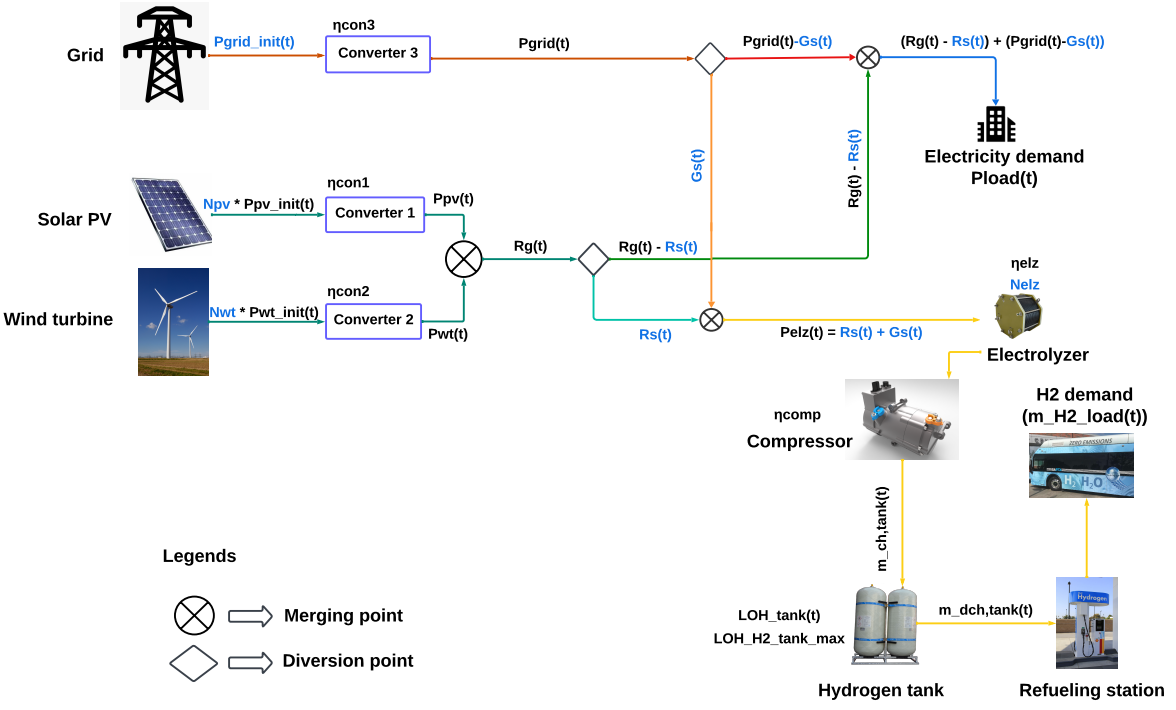

Figure 1: System architecture (blue highlighted texts represent the decision variables).

Dijon, France, has set a goal to establish itself as a leading H_2 city, focusing on the local production and consumption of decarbonized H_2 to support a zero-emission mobility strategy. Although Dijon is not the only city with such aspirations, it stands out through its concrete initiatives. The city's H_2 production primarily relies on renewable sources like solar photovoltaics, as well as electricity generated from waste incineration. By 2023, the aim was to operate 8 H_2-powered garbage collection trucks and begin transitioning the city's entire bus fleet—comprising around 27 buses—to H_2 fuel, in alignment with agreements made by Dijon Métropole, the public transportation authority, and other local partners [31]. In 2024, Dijon launched its first operational H_2 station, which has a daily production capacity of 430 kg of H_2 per day [32]. The facility is capable of refueling approximately 20 vehicles per day and is outfitted with three dispensing units delivering H_2 at 350 bars, tailored for heavy-duty vehicles like buses and trucks. Notably, the refueling process takes less than 20 minutes, contributing to improved efficiency and user convenience. The deployment of this station was structured in two distinct phases, as outlined by [31]:

(i) Northern Dijon: Establishment of 4 distribution stations to support zero-emission vehicles across the country.
(ii) Southern Dijon: Development of 175 distribution stations aimed at powering zero-emission buses throughout the community and its surrounding areas.

Among planned cases, only two H_2 production and distribution stations are currently in operation, serving both the northern and southern regions of Dijon as shown in Figure 2.

2.1. Assumptions

To effectively schedule the refueling of the bus fleet, several assumptions are made based on the case scenarios of the available facilities, using the case study of Dijon, France, as illustrated in Figure 3. These assumptions are outlined below:

1. **On-site H_2 production and consumption**: H_2 is produced and consumed on-site, primarily using renewable energy sources, with supplemental power from the electrical grid as needed.

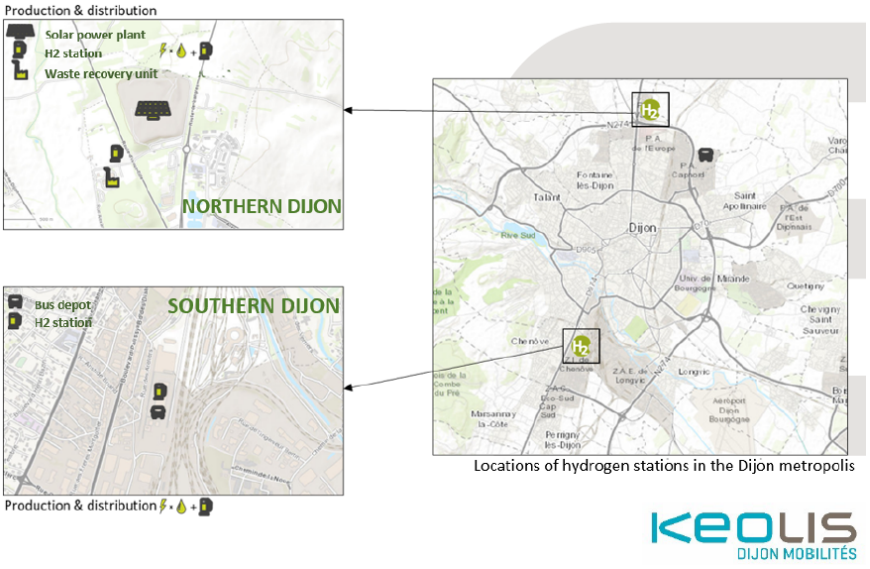

Figure 2: H_2 production and distribution station into service in Dijon by KEOLIS (retrieved from [31])

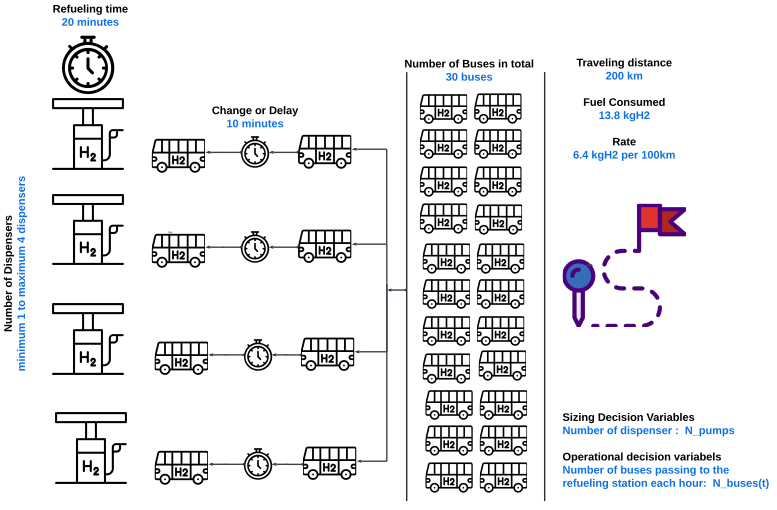

Figure 3: Diagram representing the assumptions made on the case study

2. **Daily refueling requirement**: A total of 30 buses is considered in this case study for daily refueling with a total need of 414 kg of H_2, consistent with the contract of Dijon, France [31]. The daily fuel demand is assumed constant to maintain model tractability, while additional sensitivity tests have been performed with representative summer and winter renewable profiles to verify that seasonal variations have a negligible impact on the comparative results.
3. **Consistent fuel consumption**: Each bus is assumed to need only one full refueling session per day, leading to a uniform fuel consumption pattern across the fleet. In addition, the refueling schedule is assumed to be the same every day of the year.
4. **Uniform refueling time and bus changeover**: The time required to refuel each bus, along with the delays associated with switching buses, is considered to be the same for all buses.
5. **Restricted refueling periods**: Refueling or recharging may be limited during specific times, necessitating consideration of downtime and restricted operational windows when planning refueling schedules.

6. **Compressor operation**: Compressor electricity consumption is neglected, as it accounts for less than 3–4% of the total station energy demand in typical bus refueling applications. This simplification has a negligible influence on the comparative results and overall techno-economic trends.

2.2. Other Inputs

Components	Parameters	Values	Sources
Solar PV	Module name	CECMod	[33]
	Module efficiency	17 %	
	Module Area	1.3 m²	
	Nominal Power	175 W	
	Azimuth Angle	180 degrees (South)	
	Tilt Angle	45 degrees	
	Temperature Coefficient (ψ)	-0.5072 %/°C	
	Derating Factor	0.8	
	Technical lifetime	project lifetime	assumed
WT	Module name	GE Energy 3.2-130	[34]
	Nominal Power	3.2 MW	
	Cut-in wind speed	3 m/s	
	Cut-out wind speed	25 m/s	
	Hub height	110 m	
	Rotor diameter	130 m	
	Rated wind speed	12.5 m/s	
	Roughness length	0.1	
	Technical lifetime	project lifetime	assumed
Elz	Nominal Power	2 MW	[35]
	Efficiency	66.5%	
	Technical lifetime	project lifetime	assumed
H_2 tank	Technical lifetime	project lifetime	assumed
Other	Converter efficiency (η_{conv})	95%	[36]
	Compressor efficiency (η_{comp})	75%	assumed
	Number of bus	30	assumed
	Refueling time	20 min/bus	assumed
	Demand	6.4 kg H_2/100 km	assumed
	Travel distance	200 km/bus	assumed
	Time horizon (T)	5 years, 43800 hours	multi-year
	Time step (t)	1 hour	
	Electricity purchase price [1]	Price range (France, 2019-2023)	
	Electricity carbon intensity (ϵ_{ems})	68 gCO_2/kWh (France, 2022)	[37]
	H_2 production carbon footprint	< 3.38 $kgCO_2$/kg H_2	[38]
	H_2 production carbon footprint[2]	< 3 $kgCO_2$/kg H_2	[39]

[1]The daily grid electricity prices were analyzed from August 2023 to the present, using data from "le gestionnaire du réseau de transport d'électricité français" [40].

[2]3 $kgCO_2$/kg H_2 is defined in "Delegated regulation for a minimum threshold for GHG savings of recycled carbon fuels annex" [39]

Table 3: Technical Parameters of the study

Components	$Capex$(FIXED)	$Opex$ (FIXED)	Lifetime (years)	Sources
Solar PV	120,000 €/MW	9,600 €/MW/year	20	[35]
WT	1,120,000 €/MW	14,000 €/MW/year	20	[35]
Elz	750,000 €/MW	5% of $Capex$ €/MW/year	20	[35]
H_2 Tank	57,000 €/MWh	5% of $Capex$ €/MWh/year	20	[35]
Refueling points	107,000 €	5350 €/year	20	[3]

Project lifetime is considered 20 years, discount rate for the project is taken to be 7.8% .

Table 4: Economic Parameters of the Study

This study employs solar irradiance and wind speed data sourced from the National Solar Radiation Database (NSRDB) [41] and the MERRA-2 reanalysis dataset [42], respectively. These datasets are used to generate power output profiles for solar PV and WT systems. For this purpose, the Python-based libraries pvlib [33] and windpowerlib [43] are utilized. These tools allow for detailed modeling based on parameters such as solar radiation, PV module specifications, wind turbine characteristics, wind speed, and manufacturer power curves. The solar irradiation and wind speed data are presented in Appendix A, Figures (a) and (b).

Electricity demand data for Dijon, covering the period from January 1, 2019, to December 31, 2023, is sourced from Open Data Réseaux Énergies (ODRÉ) [44]. The data reveals a peak load of 395 MW, as illustrated in Appendix A, Figure (c). In addition, historical electricity spot prices in France over the same period (2019–2023) are incorporated into the analysis, based on data provided by the French transmission system operator, RTE [40]. These price trends are depicted in Appendix A, Figure (d).

The technical and economic parameters of different components involved are presented in Table 3 and Table 4.

2.3. Optimization framework

The model formulates a single-objective optimization problem with the goal of minimizing the Total Annual Cost (TAC) over a 5-year period, equivalent to 43,800 hours of planning horizon (T), divided into hourly time steps (t). As part of the optimization process, along with all the optimal sizing of all the components such as solar PV, WT, Elz, and H_2 tank, the model also determines the optimal number of active refueling points and the number of buses refueled during each hour within a 24-hour daily cycle. These decisions are then uniformly extended across the entire 5-year horizon to ensure a cost-efficient refueling strategy. To construct the optimization framework, inputs, a set of decision variables, and operational constraints are defined, as described in the following section.

The major inputs to the optimization problem are:

(a) Meteorological data, including five-year solar irradiance and wind speed data.
(b) Five years of electricity demand and prices data.
(c) H_2 demand is assumed to be uniformly distributed across all days of five years and scheduled dynamically within the optimal cost optimization framework.
(d) The techno-economic data of all the components, i.e., PV, WT, Elz, H_2 tank, converters, compressor and H_2 refueling points.

The decision variables represented in bold italics format are given as:

(a) Numbers of solar photovoltaic panels, wind turbines, electrolyzers and refueling points ($\boldsymbol{N_{PV}}$, $\boldsymbol{N_{WT}}$, $\boldsymbol{N_{Elz}}$, $\boldsymbol{N_{pump}}$).
(b) Maximum capacity of the H_2 tank ($\boldsymbol{LOH_{H2_{tank,max}}}$) in kg.

The decision variables based on the operations represented in bold italics are given as:

(a) Grid operation ($\boldsymbol{P_{grid,init}}(t)$) in MW $\forall t \in T$.
(b) Waste of power ($\boldsymbol{P_{waste}}(t)$) in MW $\forall t \in T$.
(c) Number of buses visiting the refueling station daily at each hour $\boldsymbol{N_{buses}}(t)$ in numbers $\forall t$ for one day, i.e., 24h.
(d) $\boldsymbol{R_s(t)}$ represents the portion of renewable power allocated to the electrolyzer in MW, and $\boldsymbol{G_s(t)}$ represents the portion of grid power allocated to the electrolyzer in MW $\forall t \in T$.

The decision variables in the optimization model include both integer and continuous decision variables. The integer variables represent the sizing of key system components—-specifically, the number of solar PV panels, WT, and Elz and the number of buses refueled per hour in a day ($\boldsymbol{N_{buses}}(t)$). The number of buses to be refueled each hour in each day ($\boldsymbol{N_{buses}}(t)$) is simplified and considered the same for each day throughout the time horizon. This reduced the number of integer variables to be optimized, which aids in increasing the computational efficiency. Each component type, such as solar PV, WT, and Elz, is modeled as a standardized module with a defined nominal capacity, as detailed in Table 3. The total installed capacity of each component is calculated by multiplying the number of selected modules, denoted as $\boldsymbol{N_{PV}}$, $\boldsymbol{N_{WT}}$, and $\boldsymbol{N_{Elz}}$, respectively. Time-dependent decision variables, including grid electricity input

($\boldsymbol{P_{grid,init}}(t)$), energy from waste ($\boldsymbol{P_{waste}}(t)$), and share of renewable generation and grid to electrolyzer ($\boldsymbol{R_s}(t)$ and $\boldsymbol{G_s}(t)$), are modeled as continuous variables and optimized over the time horizon to minimize total cost. The inclusion of both integer and continuous variables makes this a Mixed-Integer Linear Programming (MILP) problem. MILP problems are generally NP-hard, meaning that they cannot be solved in polynomial time and are computationally intensive, especially as the number of integer decision variables increases. An important distinction is whether the daily H_2 demand profile based on the number of buses refueled per hour on a day ($\boldsymbol{N_{buses}}(t)$) is treated as a fixed parameter or as an additional set of integer decision variables. When treated as an integer decision variable, the choice substantially increases the problem's dimensionality: from zero integer variables (when treated as a parameter) to 24 additional integer variables (one for each hour), resulting in greater computational complexity and longer solution times.

A customized and tractable MILP problem is addressed using a fully developed optimization tool named "KLMS-OPT" [45], built on the Python-based Pyomo framework [46]. This tool is specifically designed to model and solve energy system problems, enabling practical evaluation of the solutions obtained. The general hybrid system formulation builds upon the structure introduced in [47], which is extended here to include hourly H_2 refueling scheduling, policy-based operational constraints, and a real-scale application to the Dijon case. The model is implemented in Python 3.9 and executed using the Spyder IDE, with optimization performed via the Gurobi^{TM} solver (version 10.0.1). All simulations are carried out on a personal laptop equipped with an 11th Gen Intel® Core^{TM} i5-1145G7 CPU @ 2.60GHz.

2.4. Modeling and Constraint

The comprehensive modeling approach used in this study is detailed in [47]. A complete list of model symbols, indices and variables is provided at the end of the paper. The MILP formulation includes several groups of constraints that describe the operation of the hybrid renewable–H_2 system and ensure feasibility of the sizing and scheduling problem. All constraints are linear, preserving MILP tractability. The main groups are summarized below:

2.4.1. Solar Panel Model

This model accounts for direct normal irradiance (DNI), global horizontal irradiance (GHI), and diffuse horizontal irradiance (DHI), which are extracted from the National Solar Radiation Database (NSRDB) [41] for the geographical coordinates of Dijon, France. Then the model is applied as per Badescu [48] to calculate the global irradiance $T_i(t)$ in the tilted surface of solar PV with tilt angle (θ) set at 45° given as follows:

$$G_{direct}(t) = DNI(t) \times cos(A(t)) \quad \forall t \in [0, T-1] \quad (\text{W/m}^2) \tag{1}$$

$$G_{diffused}(t) = DHI(t) \times \frac{3 + cos(2\theta)}{4} \quad \forall t \in [0, T-1] \quad (\text{W/m}^2) \tag{2}$$

$$G_{Reflected}(t) = GHI(t) \times albedo \times \frac{1 - cos(\theta)}{2} \quad \forall t \in [0, T-1] \quad (\text{W/m}^2) \tag{3}$$

$$T_i(t) = G_{direct}(t) + G_{diffuse}(t) + G_{Reflected}(t) \quad \forall t \in [0, T-1] \quad (\text{W/m}^2) \tag{4}$$

The cell temperature is expressed as :

$$T_{cell}(t) = T_{STC} + \frac{T_{NOCT} - Ta_{NOCT}}{G_{NOCT}} \times T_i(t) \quad \forall t \in [0, T-1] \quad (°\text{C}) \tag{5}$$

The PV generator efficiency is expressed as :

$$\eta_{PV}(t) = \eta_{mod} \times (1 - \psi \times (T_{cell}(t) - T_{STC})) \quad \forall t \in [0, T-1] \quad (\%) \tag{6}$$

The power output then is derived as per the existing literature [33] given as:

$$P_{PV,init}(t) = \eta_{PV}(t) \times DF \times A_{PV} \times T_i(t) \quad \forall t \in [0, T-1] \quad (\text{W}) \tag{7}$$

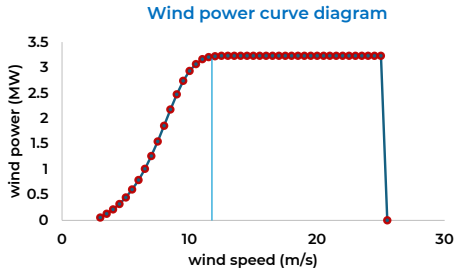

Figure 4: Wind power curve profile

2.4.2. Wind Turbine Model

The power produced by each wind turbine is predicted by using the power curve as shown in Figure 4. There are several existing models, such as the linear model, the model based on the Weibull parameter predicting wind speed distributions, and quadratic and cubic models [49], [50]. Similar to [50], the cubic model has been chosen because of its adequate fit in calculating the wind power output.

$$P_{WT,init}(t) = \begin{cases} 0, & V(t) \le V_{cin} \text{ or } V(t) \ge V_{cout} \\ P_{R_{WT}}, & V_R \le V(t) \le V_{cout} \\ P_{R_{WT}} \times \dfrac{V(t)^3 - V_{cin}^3}{V_R^3 - V_{cin}^3}, & V_{cin} \le V(t) \le V_R \end{cases} \quad \forall t \in [0, T-1] \quad \text{(MW)} \tag{8}$$

2.4.3. Grid

The grid is used as backup power to maintain the electrolyzer operation as well as satisfy the electricity need during the unavailability of renewable generation. It is considered to have unlimited capacity. The efficiency of the power converter is considered, enabling connection to the grid as depicted in Equation 9.

$$P_{grid}(t) = \boldsymbol{P_{grid,init}}(t) \times \eta_{con3} \quad \forall t \in [0, T-1] \quad \text{(MW)} \tag{9}$$

2.4.4. Total Renewable Generation

The total renewable generation, denoted as $R_g(t)$, is the combined power output from two renewable sources: wind turbines $P_{WT}(t)$ and photovoltaic panels $P_{PV}(t)$.
The power output of photovoltaic panels is given by:

$$P_{PV}(t) = P_{PV,\text{init}}(t) \times \eta_{con1} \quad t \in [0, T-1] \quad \text{(MW)} \tag{10}$$

The power output of wind turbines is given by:

$$P_{WT}(t) = P_{WT,\text{init}}(t) \times \eta_{con2} \quad t \in [0, T-1] \quad \text{(MW)} \tag{11}$$

To consider losses in the converters for both PV and WT, efficiency factors (η_{con1} for PV and η_{con2} for WT) are incorporated in Equation 10 and Equation 11. The decision variables $\boldsymbol{N_{WT}}$ and $\boldsymbol{N_{PV}}$ enable adjustment of these components, making the model adaptable for optimization studies that accurately reflect the available renewable power as given in Equation 12.

$$R_g(t) = \boldsymbol{N_{PV}} \times P_{PV}(t) + \boldsymbol{N_{WT}} \times P_{WT}(t) \quad t \in [0, T-1] \quad \text{(MW)} \tag{12}$$

2.4.5. Power balance and Energy management

As depicted in Figure 1, it is crucial to meet both the electricity demand of households and the power demand of the Elz for H_2 production. To achieve this, two time-dependent decision variables are introduced: $\boldsymbol{R_s}(t)$, representing the portion of renewable power allocated to the Elz, and $\boldsymbol{G_s}(t)$, representing the portion of grid power allocated to the Elz. When intermittent renewable sources cannot fully power the Elz, grid power is utilized to ensure its operation. The combined contribution of these two variables to satisfy the Elz power demand is formulated in equation 13.

(a) power balance in the electrolyzer side :

$$P_{Elz}(t) = \boldsymbol{R_s}(t) + \boldsymbol{G_s}(t) \quad \forall t \in [0, T-1] \quad \text{(MW)} \tag{13}$$

The remaining share is allocated to satisfy the electricity demand, as depicted in Equation 14. Surplus renewable generation occurs when renewable sources exceed demand, leading to potential waste of power ($\boldsymbol{P_{waste}}$), particularly during the maximum renewable production period.

(b) power balance in the electric load side :

$$P_{load}(t) = \big(R_g(t) - \boldsymbol{R_s}(t)\big) + \big(P_{grid}(t) - \boldsymbol{G_s}(t)\big) - \boldsymbol{P_{waste}}(t) \quad \forall t \in [0, T-1] \quad \text{(MW)} \tag{14}$$

2.4.6. Electrolyzer

With current technology development, the electrolyzer (Elz) exhibits a minimum operating point within the range of 10-50% [51]. Optimal flexibility allows the electrolyzer to operate at a minimum of 10% [51], thus establishing the minimum operational threshold (z_{min}) for the Elz in this case as 15%.
The operating power of the Elz is constrained as :

$$P_{Elz}(t) \leq \boldsymbol{N_{Elz}} \times P_{Elz_{unit,max}} \quad t \in [0, T-1] \quad \text{(MW)} \tag{15}$$

$$P_{Elz}(t) \geq \boldsymbol{N_{Elz}} \times P_{Elz_{unit,max}} \times z_{min} \quad t \in [0, T-1] \quad \text{(MW)} \tag{16}$$

The mass of H_2 produced from the electrolyzer is expressed as :

$$m_{H2_{Elz,out}}(t) = \frac{P_{Elz}(t) \times \Delta t \times \eta_{Elz}}{HHV} \quad t \in [0, T-1] \quad \text{(kg)} \tag{17}$$

The mass of produced H_2 charged to the compressed H_2 tank at the pressure of 350 bar considering the losses that occurred in the compressor is given as :

$$m_{ch}(t) = m_{H2_{Elz,\text{out}}}(t) \times \eta_{comp} \quad t \in [0, T-1] \quad \text{(kg)} \tag{18}$$

2.4.7. Hydrogen storage tank

The constraint in the H_2 tank is based on the level of H_2 in the tank ($LOH_{H2_{tank}}$) (Equation 19) which is determined at any time for each time step (t) throughout the time horizon (T). At any time step (t), the level of H_2 in the storage tank is based on the H_2 charged in the previous time step including the compressor losses which is described in Equation 20.

$$LOH_{H2_{tank}}(t) = LOH_{H2_{tank}}(t-1) + m_{ch,tank}(t) - m_{dch,tank}(t) \quad \forall t \in [1, T-1] \quad \text{(kg)} \tag{19}$$

$$m_{ch,tank}(t) = m_{H2_{Elz,\text{out}}}(t) \times \eta_{isen} \quad \forall t \in [0, T-1] \quad \text{(kg)} \tag{20}$$

H_2 tank is initialized at 50% of its total capacity, as defined in Equation 21. To ensure system reliability and maintain proper pressure, the tank's state of charge is constrained between a minimum of 50% (s_{min}) and a maximum of 100% (s_{max}), as given in Equation 22 and Equation 23. Throughout the 5-year time horizon (T), discharge from the tank is

set to exactly match the hourly H_2 demand at each time step (t), as formulated in Equation 24. This ensures a consistent balance between supply and demand. Additionally, the refueling station is assumed to operate at 350 bar, requiring no further compression.

$$LOH_{H2_{tank}}(0) = \boldsymbol{LOH_{H2_{tank,max}}} \times s_{min} \quad \text{(kg)} \tag{21}$$

$$LOH_{H2_{tank}}(t) \geq \boldsymbol{LOH_{H2_{tank,max}}} \times s_{min} \quad \forall t \in [1, T-1] \quad \text{(kg)} \tag{22}$$

$$LOH_{H2_{tank}}(t) \leq \boldsymbol{LOH_{H2_{tank,max}}} \times s_{max} \quad \forall t \in [1, T-1] \quad \text{(kg)} \tag{23}$$

$$m_{dch}(t) = m_{H2_{load}}(t) \quad t \in [0, T-1] \quad \text{(kg)} \tag{24}$$

In the second case when the H_2 demand is considered to be scheduled, constraints are added as given in the following sections.

2.4.8. Number of Buses at Refueling Station

In this scenario, it is projected that a total number of buses ($N_{bus,tot}$) will require daily refueling, contingent on the operational hours and availability of the points. The total number of buses available for refueling each day for a 24-hour of time horizon is considered to be 30. All the buses are supposed to visit the station for refueling once a day throughout the time horizon of five years, with the number of buses refueled each hour (t) optimized through a cost-effective scheduling approach. Since the daily refueling schedule is assumed to be the same each day, it leads to Equation 26. In this study, the estimation is based on the following constraint:

$$\sum_{t \text{ for one day (24h)}} \boldsymbol{N_{buses}}(t) = N_{bus,tot} \tag{25}$$

$$\boldsymbol{N_{buses}}(t) = \boldsymbol{N_{buses}}(t + 24d) \quad \forall d \in [0, 1825] \tag{26}$$

2.4.9. Station Scheduling

The number of buses ($\boldsymbol{N_{buses}}(t)$) arriving at the refueling station during a time period of 24 hours is determined by the availability of refueling points. Each refueling point can serve up to ($N_{bus,hour}$), which is set to two buses per hour in this case, given a refueling duration of 20 minutes per bus, which includes 10 minutes for transitions and other delays. This simplified assumption reflects the average observed in existing bus depots in France and was verified to remain feasible under peak-hour conditions. The values can be adjusted and tested under various scenarios, including different restricted or flexible time windows and varying numbers of buses. The same number of buses is scheduled to arrive at the station at the same times each day, consistently maintained over a five-year time horizon. The operational constraints related to pump usage and bus arrivals at the refueling station are described as follows.

$$\boldsymbol{N_{buses}}(t) \leq N_{bus,hour} \times \boldsymbol{N_{pump}}, \quad \forall t \in [0, T-1] \tag{27}$$

2.4.10. Total hydrogen demand

The total H_2 demand is calculated based on the total number of buses passing to the station hourly throughout the day. The hourly H_2 demand ($m_{H2_{load}}(t)$) is determined by multiplying the daily H_2 consumption of each bus ($D_{daily_{perbus}}$) by the number of buses operating each hour throughout a day. Additionally, the daily H_2 profile is assumed to be uniform, which enables the creation of a consistent yearly H_2 profile. A uniform profile is preferred, as it facilitates

more predictable and stable supply chain logistics, maintenance schedules, and cost estimations, thereby providing a more reliable framework compared to fluctuating yearly profiles. The constraint for the total H_2 demand is expressed as follows:

$$m_{H2_{load}}(t) = D_{daily_{perbus}} \times \boldsymbol{N_{buses}}(t), \quad \forall t \in [0, T-1] \quad \text{(kg)} \tag{28}$$

The total hourly H_2 demand corresponds to the amount of H_2 that must be discharged by the system during each hour.

2.4.11. Objective function

This study explores both single-objective minimization of Total Annual Costs (TAC) based in Net Present Value (NPV). NPV comprises capital investment ($Capex$) as presented in Equation 31 and operating and maintenance costs ($Opex$) as presented in Equation 35. $Opex$ is sometimes represented as the fraction of $Capex$ [52]. NPV is determined as the sum of $Capex$, $Opex$, and grid purchase of electricity (Pch_{grid}) as shown in Equation 29.

$$\text{NPV} = Capex_{tot} + C_{rep,tot} + Opex_{tot} + Pch_{grid} \quad (€) \tag{29}$$

The capital recovery factor (CRF) is defined as the ratio of a constant annuity to the present value of receiving that annuity for a given length of time [53] and is calculated using the real discount rate (i) over the economic lifetime of n, as shown in Equation 30.

$$CRF = \frac{i \cdot (1+i)^n}{(1+i)^n - 1} \tag{30}$$

For this study, the economic interest rate (i) is set at 7.8% over the system's economic lifetime of 20 years [54].

Capital investment is calculated based on the capital cost ($Capex$) associated with the capacity (Cap) of the components. The total capital investment of various components ($Capex_{tot}$) is presented as per equation 31. In all equations, j represents various components such as PV, WT, Elz, and H_2 tank. In this study, the number of refueling points is optimized based on the cost-optimal scheduling of H_2 refueling.

$$Capex_{tot} = \sum_j (Cap_j \times Capex_j) + (\boldsymbol{N_{pump}} \times Capex_{pump}) \quad (€) \tag{31}$$

The capacity of certain components, such as solar photovoltaic, wind turbine, and electrolyzer, is represented based on the number of units and their rated capacities, as follows:

$$Cap_{PV} = \boldsymbol{N_{PV}} \times Unit_{cap,PV} \quad \text{(MW)} \tag{32}$$

$$Cap_{WT} = \boldsymbol{N_{WT}} \times Unit_{cap,WT} \quad \text{(MW)} \tag{33}$$

$$Cap_{Elz} = \boldsymbol{N_{Elz}} \times Unit_{cap,Elz} \quad \text{(MW)} \tag{34}$$

Operation and maintenance cost is calculated based on the O&M cost ($Opex$) associated with the capacity (Cap) of the components. The total capital investment of various components ($Opex_{tot}$) is presented as per Equation 35.

$$Opex_{tot} = \sum_j ((Cap_j \times Opex_j) + (\boldsymbol{N_{pump}} \times Opex_{pump})) \times \frac{1}{CRF} \quad (€) \tag{35}$$

The grid import cost refers to the expense incurred from purchasing energy from the grid, which is determined by the applicable hourly tariff or purchase rate throughout the time step ($GPR(t)$). It is given by the expression as follows:

$$Pch_{grid} = \sum_{0}^{T-1} P_{grid}(t) \times GPR(t) \times \frac{1}{CRF} \quad \forall t \in [0, T-1] \quad (€) \tag{36}$$

TAC then is calculated as shown in Equation 37.

$$\text{TAC} = \text{NPV} \times CRF \quad (€/\text{year}) \tag{37}$$

In which the annuity is calculated by considering the present value of the project using CRF.

2.5. Indicators

Based on the optimization results, key technical and environmental indicators are defined to assess system performance. These focus on green H_2 production through electrolysis and efficient electricity use. Indicators include renewable and grid energy shares, energy distribution to electrolyzers and loads, Levelized Cost of H_2 (LCOH), and CO_2 emissions per kg of H_2 produced and per unit of grid import.

2.5.1. Energy Indicators

Energy indicators are essential for evaluating the roles of solar PV, WT, and grid imports in meeting electricity and electrolyzer demands. These metrics highlight how much renewable energy contributes to H_2 production and the system's dependence on grid power. The key energy indicators include:

(i) Proportion of renewable share of energy to electrolyzer

$$R_{Rg,Elz} = \frac{\sum_0^{T-1} \boldsymbol{R_s}(t) \cdot \Delta t}{\sum_0^{T-1} P_{Elz}(t) \cdot \Delta t} \quad t \in [0, T-1] \tag{38}$$

(iii) Proportion of grid share of energy to electrolyzer

$$R_{grid,Elz} = \frac{\sum_0^{T-1} \boldsymbol{G_s}(t) \cdot \Delta t}{\sum_0^{T-1} P_{Elz}(t) \cdot \Delta t} \quad t \in [0, T-1] \tag{39}$$

2.5.2. Economic Indicator

Levelized Cost of H_2 (LCOH) is a key metric that measures the average cost of producing one kilogram of H_2 over the lifetime of a production facility. It is usually expressed in units of currency per kilogram of H_2, such as €/kg H_2. LCOH is calculated based on the share of energy allocated to H_2 production, providing a more accurate measure of the cost to produce H_2.

(i) LCOH in €/kg H_2

$$LCOH = \frac{R_{Elz,etot} \times TAC}{\sum_0^{T-1} m_{H2_{Elz,out}}(t)} \quad \forall t \in [0, T-1] \quad (€/\text{kg } H_2) \tag{40}$$

$R_{Elz,etot}$ indicates proportion of the electrolyzer demand to the total energy (including renewable generation and grid import)

$$R_{Elz,etot} = \frac{\sum_0^{T-1} P_{Elz}(t) \cdot \Delta t}{\sum_0^{T-1} R_g(t) \cdot \Delta t + P_{grid}(t) \cdot \Delta t} \quad t \in [0, T-1] \tag{41}$$

2.5.3. Environmental Indicators

This study evaluates the carbon footprint of H_2 production, denoted as $CO_{2,fprint,H2}$, based on emissions from grid electricity use. The key factor influencing this metric is the grid's carbon intensity, ϵ_{ems}, over the operational period.

(i) Carbon footprint of grid import of electricity in Mtonne CO_2/year

$$CO_{2,fprint,elec} = \sum_{0}^{T-1} P_{grid}(t) \cdot \Delta t \cdot \epsilon_{ems} \quad t \in [0, T-1] \tag{42}$$

(ii) Carbon ratio of H_2 production in $kgCO_2/kgH_2$

$$CO_{2,fprint,H2} = \frac{\sum_{0}^{T-1} \boldsymbol{G_s}(t) \cdot \Delta t \cdot \epsilon_{ems}}{\sum_{0}^{T-1} m_{H2_{Elz,out}}(t)} \quad t \in [0, T-1] \tag{43}$$

3. Results and discussions

The results obtained from the resolution of the formulated optimization problem are discussed under the following two scenarios:

1. **Flexible optimized scenario:**
   Allows refueling at any time throughout the day. This flexibility enables optimization based on electricity prices and renewable energy availability, improving overall system efficiency.
2. **Restricted optimized scenario:**
   Limits refueling to the early morning window from 3h to 7h before buses begin service. This reflects operational constraints to ensure fleet readiness.

3.1. Hydrogen refueling profile

The study demonstrates that a flexible refueling schedule for the H_2 bus fleet can significantly improve both the economic and environmental performance of the energy system. This approach aligns refueling activities with periods of lower electricity demand and reduced electricity prices, primarily during nighttime hours (1h–6h) and midday (11h–17h). During the night, around 9 out of 30 buses are refueled when grid demand is low and electricity prices are typically at their minimum. During the day, 13 buses are scheduled for refueling to coincide with peak renewable generation, as shown in Figure 5a. This scheduling strategy demonstrates that prioritizing bus refueling during off-peak hours not only minimizes H_2 production costs—leveraging lower electricity prices and reduced grid demand—but also ensures more economical operation of the energy system. First, by operating the electrolyzer during off-peak hours, the system avoids high time-of-use tariffs and peak demand charges, reducing operational costs. Second, refueling during times of high renewable availability allows greater use of low-cost, zero-emission electricity, minimizing dependence on carbon-intensive grid imports. As a result, the flexible strategy not only reduces the cost of H_2 production but also supports more sustainable and decarbonized operation, enhancing the overall economic viability of the system.

In contrast, the restricted refueling scenario confines all refueling activity to a narrow window between 3h and 7h, just before the buses begin operation. This results in a uniform hourly distribution, with 6 buses refueled per hour, as depicted in Figure 5b. Consequently, this leads to higher energy costs, making the system less flexible and economically efficient.

3.2. Sizing

While the capacities of solar PV of 211 MW and wind turbines of 349 MW remain consistent across all cases as shown in Table 5, significant differences emerge in the sizing of other key system components—electrolyzers, refueling points, and H_2 storage capacity. The flexible scheduling scenario allows for optimized, cost-effective refueling distributed throughout the day. As a result, only one electrolyzer and one refueling point are sufficient, while the H_2 storage capacity is drastically reduced to 90.29 kg, as shown in Figure 6. This lower capacity is fully compliant with the French ICPE 4715 regulation (Arrêté du 13 juillet 2017), which limits on-site H_2 storage to 100 kg for small-scale stations [55]. The flexibility in scheduling enables a more balanced system operation, minimizes component oversizing,

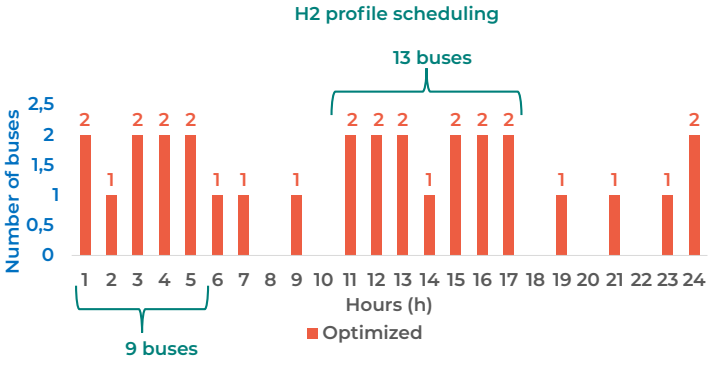

(a) Flexible optimized daily refueling profile

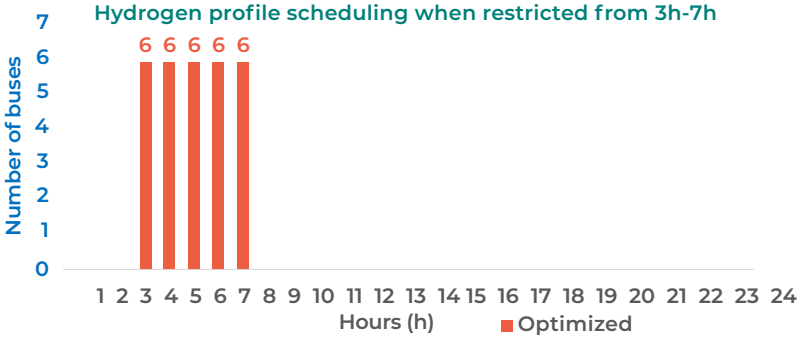

(b) Restricted optimized daily refueling profile

Figure 5: Comparison of optimized daily refueling profiles under flexible and restricted scheduling

and significantly reduced the cost.

The restricted scheduling scenario, which limits refueling to a 3h–7h morning window, lies between the other two in terms of system demand. In this case, three electrolyzers and three refueling points are required to ensure fleet readiness, and the storage level largely exceeds the 100 kg regulatory threshold, as presented in Figure 6, highlighting that such an operating policy would not be legally compliant under current French regulations and would entail major permitting and safety implications. Overall, the flexible case proves to be the most efficient in terms of component sizing and regulatory compliance.

As shown in Table 5, the system configurations involve substantial renewable capacities—approximately 349 MW of PV and 211 MW of wind power—with up to three electrolyzers and pumps and a maximum hydrogen storage capacity of 714 kg in the restricted case. Although these values appear large for an urban H_2 charging station, they result from the optimization framework that simultaneously considers the region's electricity demand, which peaks at 395 MW,

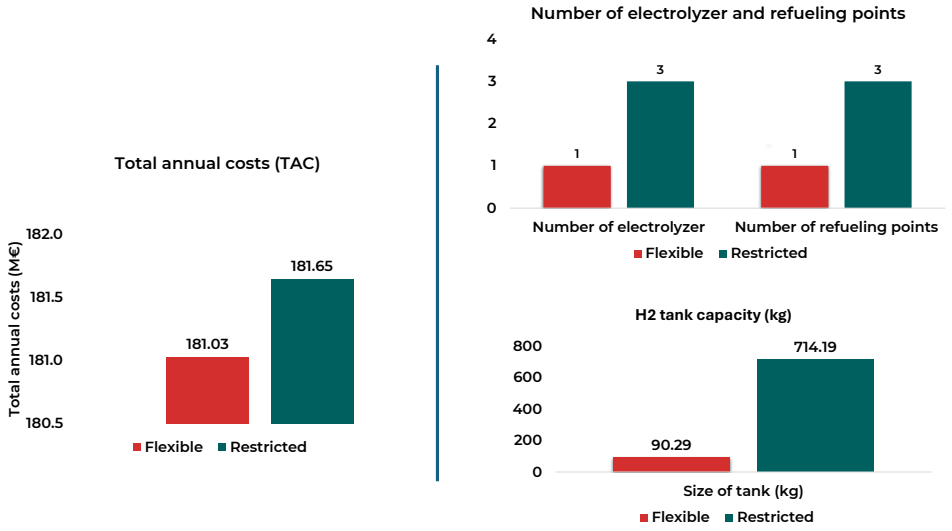

Figure 6: Sizing and cost comparison between flexible and restricted daily optimized scenario

Case Study	Cap_{PV} (MW)	Cap_{WT} (MW)	N_{Elz}	N_{pump}	$LOH_{H2_{tank,max}}$ (kg)	LO (PV) w.r.t Dijon (%)	LO (WT) w.r.t Dijon (%)	LO (WT) w.r.t BFC (%)	Runtime (minutes)
Flexible	349.2	211.2	1	1	90.29	6.42	66.24	0.06	19.87
Restricted	349.4	211.2	3	3	714.19	6.42	66.24	0.06	5.32

Wind direction: 3 × rotor diameter (130 m) [56] (within environmental framework)
Crosswind spacing: 8 × rotor diameter (130 m) [56] (within environmental framework)
Area of Dijon: 4041 hectares (ha) [57]
w.r.t: with respect to
LO: Land Occupancy
BFC: Region Bourgogne–Franche–Comté, France

Table 5: System configuration and land use for flexible vs. restricted case.

alongside the comparatively small H_2 demand corresponding to a fleet of 30 buses. Consequently, the overall system scales to a regional energy level, even though only a limited share of the PV and WT installations would actually contribute to H_2 production. In practice, such renewable capacities would not be located within the urban area of Dijon but rather distributed across the Bourgogne–Franche–Comté (BFC) region, France, which already comprises about 327.95 MW of installed wind capacity near Dijon [58], while within the city, smaller projects such as the 15 MW Valmy solar park illustrate the realistic urban potential [58]. Moreover, the required spacing of wind turbines—about three rotor diameters (130 m) in the prevailing wind direction and eight diameters crosswind—renders their installation within city limits impractical due to space, visual, and noise constraints. Therefore, the wind generation in the model should be understood as regional renewable input rather than local urban installations. Finally, H_2 storage also faces practical limitations: while the flexible case's 90 kg storage is technically manageable, the restricted case's 714 kg capacity would be economically and operationally challenging in an urban environment given hydrogen's low volumetric energy density, flammability, and safety requirements. Nevertheless, H_2 refueling infrastructure for buses is designed to meet strict international safety standards right now, and the associated risks are well controlled through containment, ventilation, and monitoring systems, as an 860 kg of H_2 storage tank is already installed in Pau, France [58] as an example. Overall, while the model's assumptions are appropriate for capturing system-level interactions,

real-world implementation would depend on regional renewable generation, limited on-site hydrogen production, and robust safety and permitting frameworks.

3.3. Indicators

Considering the economic indicator—Total Annual Cost —In comparison, flexible optimization of the H_2 refueling schedule to better align with operational requirements leads to annual cost savings corresponding to a 0.35% reduction in TAC over the system's lifetime, including 66.67% reduction in capital investment ($Capex$) of the refueling station, as illustrated in the flexible optimized scenario of Figure 6. This highlights the economic benefit of adjusting the refueling schedule, offering decision-makers valuable insights into how optimized scheduling can reduce overall costs. The improvement is primarily due to the flexibility imposed in the refueling window, which resulted in a lower number of system components, such as electrolyzers and refueling points, as presented in Figure 6 and Table 6.

The levelized cost of H_2 shows slight variations across the different scenarios. When the H_2 profile is flexibly scheduled throughout the day, the LCOH is obtained with €5.76/kg H_2, as shown in the flexible optimized scenario in Figure 7. However, in the restricted optimized scenario—where H_2 refueling is limited to specific early morning hours—the LCOH returns to €5.78/kg H_2. Despite the small differences in LCOH, an important question arises: is an LCOH above €5/kg H_2 acceptable, especially when the long-term target is to reduce the cost to below €2/kg H_2 [59]? Achieving this lower price point requires very specific conditions, including a system heavily dependent on grid imports in the case of France with lower grid electricity prices.

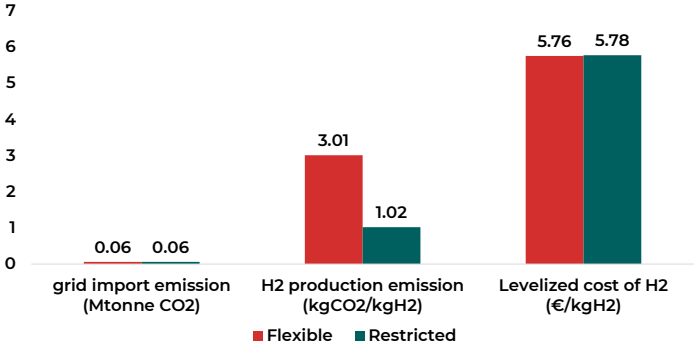

Figure 7: Indicators comparison between flexible and restricted daily optimized scenario

As shown in Figure 8, the flexibly optimized scenario, which allows refueling to occur at any time throughout the day, creates a continuous hourly demand for H_2. To keep H_2 production running without interruption, the system needs a steady and reliable electricity supply. This is especially important because of the imposed constraint to maintain at least 50% of the H_2 in the tank throughout all the time periods. Since renewable energy is intermittent, it can't always meet the requirement of steady electrolyzer operation. As a result, the system increasingly depends on grid electricity. In the flexible optimized case, this reliance on the grid lowers the share of renewable energy used for H_2 production to just 25%, relying more on grid import. In the restricted scenario, where the refueling activity is scheduled within the 3h-7h window, the renewable share for H_2 production increased to 75%, as illustrated in Figure 8.

Under the flexible optimized scenario, where H_2 demand is spread continuously throughout the day, the system relies more heavily on grid electricity. This leads to an increase in emission, rising to 3.01 $kgCO_2/kgH_2$, as shown in the flexible case in Figure 7. The emission in the flexible scenario remains just above the 3 $kgCO_2/kgH_2$ threshold defined in EU regulations for low-carbon H_2 [39]; this is largely due to the high share of nuclear energy in France's power mix. This ultimately indicates that even when the system relies entirely on the grid, the H_2 produced is decarbonized.

The outcomes underscore the effectiveness of the flexible and restricted optimized scenarios in leveraging renewable energy for H_2 production. The outcome highlights the environmental advantages of confining bus refueling activities

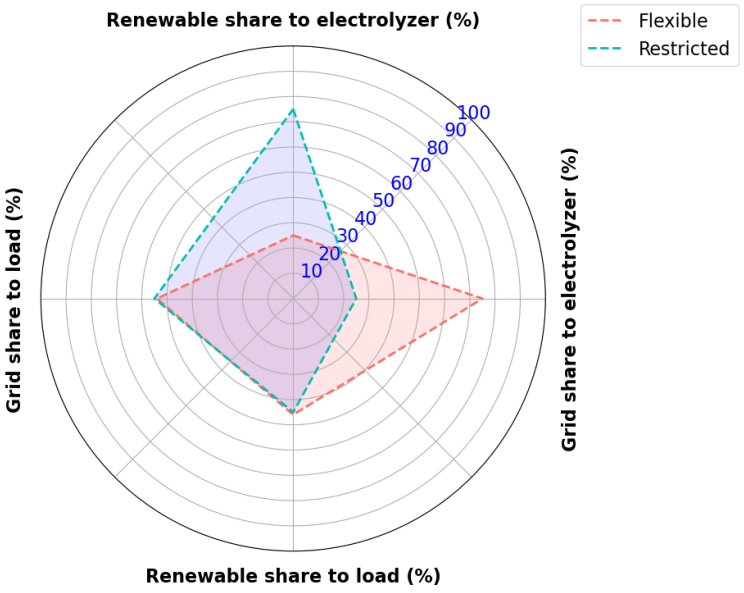

Figure 8: Share of energy comparison between flexible and restricted daily optimized scenario

Case Study	Rg→Elz (%)	Grid→Elz (%)	Rg→PL (%)	Grid→PL (%)	Elec. Emis (MTonne)	H_2 Emis ($kgCO_2/kgH_2$)	LCOH (€/kg)	TAC (€)	Waste (%)
Flexible	25.27	74.73	45.56	54.44	0.06	3.01	5.76	181.03	7.25
Restricted	74.66	25.34	45.28	54.72	0.06	1.02	5.78	181.65	7.22

PL: Power Load
Emis: Emission

Table 6: Performance comparison of flexible vs. restricted case.

to a specific time frame, especially in the early morning hours before bus services commence. This approach with restricted time is found to maximize the integration of renewable energy for the electrolyzer operation into the system, making it a viable and sustainable choice for decarbonizing transportation. In addition, from the logistic perspective, it is better to refuel the bus before the service in the morning so that it will be easy for the bus company to make a plan for the tour of the bus. When refueling activity is set or distributed during the day, finding and planning bus hours presents additional difficulty to the bus company. From a social perspective, the requirement for staff readiness at the refueling station between 3h and 7h in the early morning poses operational challenges and potential impacts on employees' work schedules.

3.4. Solution Approach and Computational Performance

In the flexible and restricted refueling optimization scenarios, the complexity of the problem increases significantly. Over 25 additional integer decision variables are introduced to model the number of buses refueling per day and the number of required refueling points. This increase in integer variables makes the problem much harder to solve—it now fits the classic NP-hard definition associated with MILP problems, where the solution space grows exponentially with the number of discrete variables. To handle these more complex cases, Gurobi likely combines the Barrier method with advanced MILP techniques such as Branch-and-Bound. These methods are known for their effectiveness in handling

Number	Initial	Flexible optimized	Restricted optimized
Objective	1	1	1
Constraints	788417	832256	832256
Variables	569420	613259	613259
Binary variables	0	0	0
Integer variables	3	28	28
Continuous variables	569417	613231	613231
Nonzeros	1897834	1839343	1839324
Runtime (seconds)	296	1192.2055 (19.87 min)	319.0160 (5.32 min)

Table 7: Optimization and computational details

large MILPs, though they can be computationally intensive. As a result, the runtime increased to approximately 19 minutes and 52 seconds for the flexible case as presented in Table 7. However, the runtime significantly decreased to about 5 minutes and 19 seconds in the restricted case because of the tighter bounds on the refueling window (limited to 3h-7h), which greatly reduced the feasible solution space.

Initially, binary variables were used to model the on/off operational status of the electrolyzers. However, this approach resulted in prohibitively long runtimes—extending to several days in some cases. Upon closer analysis, it was observed that electrolyzers predominantly operated at either full or minimal capacity throughout the time horizon. As a result, the model was reformulated to treat the electrolyzer operation as continuous, thereby eliminating binary variables. This adjustment drastically reduced computational time—bringing the simulation down from days to just seconds—without compromising the quality of the results. These findings highlight the importance of careful modeling decisions. The way constraints are formulated and how decision variables are implemented can have a profound impact on the computational performance of the optimization model. Ultimately, the choice of model formulation must align with the study's goals, requiring a balance between computational feasibility and the level of modeling accuracy desired by the decision-maker.

4. Conclusion

The study focused on determining the optimal H_2 refueling profile for a fleet of 30 H_2 buses considering the H_2 vehicle contract of Dijon, France, with an emphasis on cost optimization, and analyzing the various environmental impacts, above all the emissions associated with the grid import and H_2 production. By incorporating contractual data on bus fleet, operations and assumptions such as the distance traveled, fuel consumption per trip, and scheduling constraints, the analysis aimed to refine system components, optimize operations, and identify the most cost-effective refueling hours. Flexible and restricted scheduling of refueling profiles is explored within a time horizon of 43,800 hours at an hourly time step. This approach leveraged renewable energy, resulting in significant environmental benefits, including reduced CO_2 emissions and a lower LCOH. A subsequent analysis of a cost-optimal refueling strategy, distributed throughout the day and mentioned as a flexible optimized scenario, performed which revealed cost savings of 0.35% per year compared to a restricted profile downsizing the H_2 storage which eases the implementation of the system installation under 100 kg, excluding the need for authorization in the case of France. Nevertheless, it leads to increased dependency on the grid and associated emissions. In addition, when the refueling activity is set or distributed during the day, finding and planning the bus hours presents additional difficulty to the bus company from the logistic perspective.

Furthermore, scheduling of H_2 profile based on the restricted H_2 profile within the 3h–7h time frame is considered, which ultimately resulted in achieving small cost benefits while maximizing renewable energy utilization and enhancing decarbonization in H_2 production. However, a critical consideration lies in the social aspect—the availability of employees during early morning hours to facilitate the refueling process. This comprehensive analysis highlighted the trade-offs between cost efficiency and environmental performance, demonstrating that the restricted refueling scheduling of the H_2 refueling profile is more effective from the economic and emission points of view. However, the scheduling of H_2 refueling profiles, both throughout the day and within the restricted 3h–7h period, offered a holistic approach for evaluating the impacts of optimized refueling strategies on economic and environmental indicators. In addition, the KLMS-OPT tool allows for rapid testing of alternative scenarios, taking into account different time period

restrictions or scheduling profiles across the entire time horizon. From an optimization perspective, the computational efficiency of the developed tool is remarkable, as it resolves the problem within 20 minutes across all case scenarios, thanks to the reduction in integer variables and the implementation of tight constraints. The simulator is designed to be adaptable, enabling users to tailor it according to the specific requirements of their study. Overall, the proposed MILP framework explicitly couples system sizing and hourly refueling operations, providing actionable insights for H_2 station planning at city scale. Its main advantages lie in this integrated formulation and in its computational tractability for large instances. The current version nevertheless relies on simplified service-time representation and deterministic daily demand replication, which could be relaxed in future stochastic or multi-day extensions.

Although this study focused on two primary scenarios—a flexible refueling schedule and a restricted time window between 3h-7h—the developed optimization tool is inherently flexible and can accommodate a wide range of alternative scheduling strategies. This includes testing various restricted time frames, both before and after the bus fleet's service hours, to identify cost-optimal refueling windows under different operational conditions. In the current analysis, a uniform daily refueling profile is assumed across the entire 43,800-hour time horizon. While this assumption simplifies the modeling and ensures computational tractability, future work could extend the analysis by incorporating dynamic, time-varying refueling demands, which would increase the realism of the model but also introduce additional computational complexity. Moreover, the study is limited to the refueling of a fixed fleet of 30 H_2 buses. Expanding the scope to include heterogeneous or randomly arriving H_2-powered vehicles, such as cars or trucks, would provide a more comprehensive assessment of real-world refueling station operations. This would involve modeling stochastic demand patterns and vehicle arrival times, offering deeper insights into system performance under uncertainty. Finally, while the current study primarily focused on the development and validation of the optimization framework for H_2 refueling demand scheduling in the case of Dijon, France, future work will consider a comprehensive sensitivity and uncertainty analysis aimed at establishing the robustness of the results against fluctuating environmental, technical, and economic conditions.

Nomenclature

Parameters

θ	Tilt angle (°)
$albedo$	Albedo
A	Angle of incidence (radian)
A_{PV}	Area of PV (m²)
DF	Derating Factor
DHI	Direct Horizontal Irradiation (W/m^2)
DNI	Direct Normal Irradiation (W/m^2)
GHI	Global Horizontal Irradiation (W/m^2)
G_{NOCT}	Global irradiance at nominal operating cell temperature (W/m^2)
G_{direct}	Direct Irradiation (W/m^2)
$G_{diffused}$	Diffused Irradiation (W/m^2)
$G_{Reflected}$	Reflected Irradiation (W/m^2)
$P_{R_{WT}}$	Wind turbine rated power output (MW)
$P_{PV,init}$	Photovoltaic panel power initial (MW)
$P_{WT,init}$	Wind turbine power initial (MW)
$T_{a,NOCT}$	Ambient temperature at nominal operating cell temperature (°C)
T_{cell}	Photovoltaic module cell temperature (°C)
T_{NOCT}	Nominal Operating Cell Temperature (°C)
T_{STC}	Cell temperature at standard conditions (°C)
T_i	Total Irradiation (W/m^2)
V_{cin}	Cut-in wind speed (m/s)
V_{cout}	Cut-out wind speed (m/s)
V_R	Rated wind speed (m/s)
V_t	Wind speed (m/s)
η_{mod}	PV module efficiency
η_{PV}	PV generator efficiency
ψ	Maximum Power Temperature Coefficient (%/°C)
η_{con3}	Converter efficiency 3 (%)
η_{Elz}	Electrolyzer efficiency (%)
HHV	Higher heating value of H_2 (MJ/kg)
$m_{H2_{load}}$	Mass of H_2 load (kg)

$m_{dch,tank}$	Mass of H_2 discharged (kg)
η_{isen}	Compressor isentropic efficiency (%)
$P_{Elz_{unit,max}}$	Electrolyzer rated power (MW)
z_{min}	Electrolyzer minimum operation threshold (%)
s_{min}	Minimum level of H_2 in the tank (%)
s_{max}	Maximum level of H_2 in the tank (%)
i	Discount rate (%)
n	Project lifetime (years)
$Capex$	Capital Investment (€/Unit)
$Opex$	Operation and maintenance cost (€/Unit/year)
Cap	Capacity of the component (Unit)
Cap_j	Installed capacity of the components
ϵ_{ems}	Electricity carbon intensity ($kgCO_2$-eq/Unit)
$CO2_{ems,grid}$	Carbon emission from the grid import of energy ($kgCO_2$-eq)
$N_{bus,tot}$	Total number of bus fleet
$N_{bus,hour}$	Maximum number of bus in the pump per hour
$D_{daily_{perbus}}$	Total daily H_2 demand per bus

Sets

Δt	Interval of time between two time steps
$\boldsymbol{J}$	Set of components, $j \in \boldsymbol{J}$
$\boldsymbol{T}$	Time horizon
t	time step within time horizon, $t \in \{0, \dots, \boldsymbol{T}-1\}$

Sizing Decision Variables

$\boldsymbol{N_{PV}}$	Number of solar photovoltaic panels
$\boldsymbol{N_{WT}}$	Number of wind turbines
$\boldsymbol{N_{Elz}}$	Number of electrolyzers
$\boldsymbol{N_{pump}}$	Number of dispensers
$\boldsymbol{LOH_{H2_{tank,max}}}$	Capacity of H_2 tank (kg)

Operation Decision Variables

$\boldsymbol{P_{grid,init}}$	Imported grid power (MW)
$\boldsymbol{P_{waste}}$	Waste power (MW)
$\boldsymbol{N_{buses}}$	Number of buses passing to refueling station
$\boldsymbol{R_s}$	Share of renewable energy (MW)
$\boldsymbol{G_s}$	Share of grid import (MW)

Dependent Operation Variables

P_{PV}	Photovoltaic panel power (MW)
P_{WT}	Wind turbine power (MW)
R_g	Total renewable generation (MW)
P_{grid}	Total grid import (MW)
P_{Elz}	Input power to the electrolyzer (MW)
$m_{H2_{Elz,out}}$	Mass of produced H_2 (kg)
$m_{ch,tank}$	Mass of H_2 charged (kg)
$LOH_{H2_{tank}}$	H_2 tank level (kg)
$m_{H2_{load}}$	Mass of H_2 load (kg)

CRediT authorship contribution statement

Sarad Basnet: Conceptualization of this study, Data curation, Methodology, Software, Writing, Original draft, Review & editing. **Karine Deschinkel:** Conceptualization of this study, Methodology, Software, Writing, Review & editing, Supervision. **Luis Le Moyne:** conceptualization of this study, Methodology, Writing, Review & editing, Supervision. **Marie Cécile Péra:** Conceptualization of this study, Methodology, Writing, Review & editing, Supervision.

Acknowledgment

This work has been supported by the EIPHI Graduate School (contract ANR-17-EURE-0002), by the Region Bourgogne Franche-Comté, and by the ISITE BFC (contract ANR-15-IDEX-003).

Appendix A

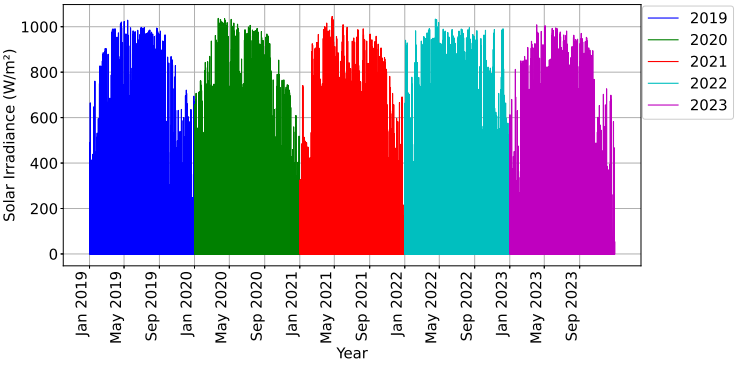

(a) Solar irradiance from 2019 to 2023 in Dijon, France.

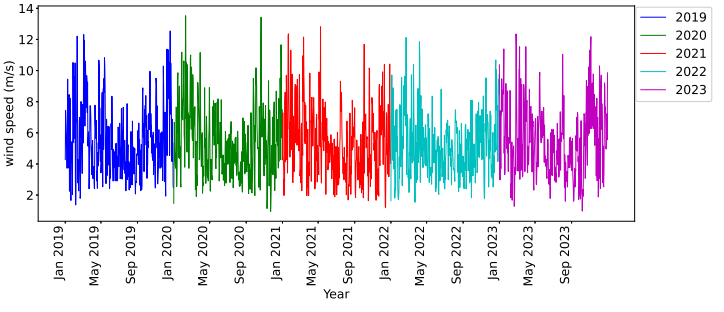

(b) Wind speed from 2019 to 2023 in Dijon, France.

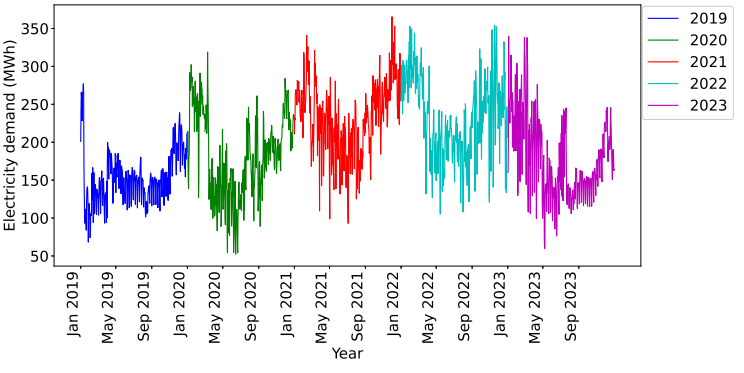

(c) Electricity demand from 2019 to 2023 in Dijon, France.

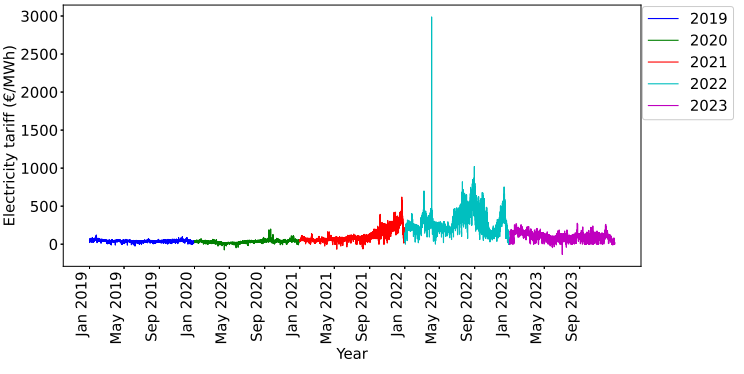

(d) Electricity tariff from 2019 to 2023 in France.

References

[1] C. Mayet, A. Hankour, B. Lakhdari, S. Rezoug, A. Bouscayrol, P. Delarue, C. Brocart, Estimation of the energy consumption and ghg emission of a public rail transport system in france combining tramways and metros for daily commuting, in: 2024 IEEE Vehicle Power and Propulsion Conference (VPPC), IEEE, 2024, pp. 1–6.

[2] P. Soszynska, H. Saleh, H. Kar, L. V. Iyer, C. Viana, N. C. Kar, Driving the future: an analysis of total cost of ownership for electrified vehicles in north america, World Electric Vehicle Journal 15 (11) (2024) 492.

[3] F. Grüger, L. Dylewski, M. Robinius, D. Stolten, Carsharing with fuel cell vehicles: Sizing hydrogen refueling stations based on refueling behavior, Applied energy 228 (2018) 1540–1549.

[4] S. I. Pérez-Uresti, G. Gallardo, D. K. Varvarezos, Strategic investment planning for the hydrogen economy–a mixed integer non-linear framework for the development and capacity expansion of hydrogen supply chain networks, Computers & Chemical Engineering 179 (2023) 108412.

[5] G. I. Prokopou, J. M. Faust, A. Mitsos, D. Bongartz, Cost-optimal design and operation of hydrogen refueling stations with mechanical and electrochemical hydrogen compressors, Computers & Chemical Engineering 192 (2025) 108862.

[6] J. Gao, H. Wu, L. Chen, Q. Meng, J. Liu, Research on optimization layout of hydrogen refueling facility network based on renewable energy hydrogen production mode, Energy 296 (2024) 131166.

[7] R. Caponi, A. M. Ferrario, L. Del Zotto, E. Bocci, Hydrogen refueling stations and fuel cell buses four year operational analysis under real-world conditions, International Journal of Hydrogen Energy 48 (54) (2023) 20957–20970.

[8] L. McLoughlin, Nearly 80% of global hydrogen refueling stations are located in just five countries (2025).
URL https://www.evcandi.com/news/nearly-80-global-hydrogen-refueling-stations-are-located-just-five-countries

[9] T. S. Le, T. N. Nguyen, D.-K. Bui, T. D. Ngo, Optimal sizing of renewable energy storage: A techno-economic analysis of hydrogen, battery and hybrid systems considering degradation and seasonal storage, Applied Energy 336 (2023) 120817.

[10] R. Vandenberghe, G. Humbert, H. Cai, B. P. Koirala, G. Sansavini, P. Heer, Optimal sizing and operation of hydrogen generation sites accounting for waste heat recovery, Applied Energy 380 (2025) 125004.

[11] J. O. Robles, C. Azzaro-Pantel, A. Aguilar-Lasserre, Optimization of a hydrogen supply chain network design under demand uncertainty by multi-objective genetic algorithms, Computers & Chemical Engineering 140 (2020) 106853.

[12] F. Grueger, O. Hoch, J. Hartmann, M. Robinius, D. Stolten, Optimized electrolyzer operation: Employing forecasts of wind energy availability, hydrogen demand, and electricity prices, International Journal of Hydrogen Energy 44 (9) (2019) 4387–4397.

[13] R. M. Rizk-Allah, I. A. Hassan, V. Snasel, A. E. Hassanien, An optimal standalone wind-photovoltaic power plant system for green hydrogen generation: Case study for hydrogen refueling station, Results in Engineering 22 (2024) 102234.

[14] M. Gökçek, N. Paltrinieri, Y. Liu, E. Badia, A. Ş. Dokuz, A. Erdoğmuş, B. B. Urhan, Ö. Yoldaş, Optimum sizing of hybrid renewable power systems for on-site hydrogen refuelling stations: Case studies from türkiye and spain, International Journal of Hydrogen Energy 59 (2024) 715–729.

[15] L. Zhao, J. Brouwer, Dynamic operation and feasibility study of a self-sustainable hydrogen fueling station using renewable energy sources, International journal of hydrogen energy 40 (10) (2015) 3822–3837.

[16] L. Viktorsson, J. T. Heinonen, J. B. Skulason, R. Unnthorsson, A step towards the hydrogen economy—a life cycle cost analysis of a hydrogen refueling station, Energies 10 (6) (2017) 763.

[17] Y. Li, F. Liu, K. Chen, Y. Liu, Technical and economic analysis of a hybrid pv/wind energy system for hydrogen refueling stations., Energy (2024) 131899.

[18] D. Lu, J. Sun, Y. Peng, X. Chen, Optimized operation plan for hydrogen refueling station with on-site electrolytic production, Sustainability 15 (1) (2022) 347.

[19] M. Tostado-Véliz, P. Horrillo-Quintero, P. García-Triviño, L. M. Fernández-Ramírez, F. Jurado, Optimal sitting and sizing of hydrogen refilling stations in distribution networks under locational marginal prices, Applied Energy 374 (2024) 124075.

[20] J. Yang, F. Yu, K. Ma, B. Yang, Z. Yue, Optimal scheduling of electric-hydrogen integrated charging station for new energy vehicles, Renewable Energy 224 (2024) 120224.

[21] L. Zhen, J. Wu, Z. Yang, Y. Ren, W. Li, Hydrogen refueling station location optimization under uncertainty, Computers & Industrial Engineering 190 (2024) 110068.

[22] Y. Du, D. Jia, X. Li, A robust dynamic hydrogenation network layout model considering station capacity expansion and flexible transportation modes, International Journal of Hydrogen Energy 58 (2024) 223–238.

[23] Y. Zhang, W. Zhang, Y. He, H. Zhang, W. Chen, C. Yang, H. Dong, Capacity optimization of renewable-based hydrogen production–refueling station for fuel cell electric vehicles: A real-project-based case study, Sustainability 17 (16) (2025) 7311.

[24] P. Ju, F. Liu, Optimization of the operation of integrated hydrogen refueling stations for wind solar hydrogen storage considering hydrogen production efficiency characteristics, in: Journal of Physics: Conference Series, Vol. 3084, IOP Publishing, 2025, p. 012077.

[25] B. Şafak, A. Çiçek, Multi-objective optimal energy management strategy for grid-interactive hydrogen refueling stations in rural areas, Sustainability 17 (6) (2025) 2663.

[26] A. Cicek, Multi-objective operation strategy for a community with ress, fuel cell evs and hydrogen energy system considering demand response, Sustainable Energy Technologies and Assessments 55 (2023) 102957.

[27] H. Ryu, D. Lee, J. Shin, M. Song, S. Lee, H. Kim, B.-I. Kim, A web-based decision support system (dss) for hydrogen refueling station location and supply chain optimization, International Journal of Hydrogen Energy 48 (93) (2023) 36223–36239.

[28] S. Bae, E. Lee, J. Han, Multi-period planning of hydrogen supply network for refuelling hydrogen fuel cell vehicles in urban areas, Sustainability 12 (10) (2020) 4114.

[29] J. Kurtz, T. Bradley, E. Winkler, C. Gearhart, Predicting demand for hydrogen station fueling, International Journal of Hydrogen Energy 45 (56) (2020) 32298–32310.

[30] N. Isaac, A. Saha, Analysis of refueling behavior of hydrogen fuel vehicles through a stochastic model using markov chain process, Renewable and Sustainable Energy Reviews 141 (2021) 110761.
[31] T. Fontaine, Hydrogen project in dijon, https://www.sustainable-bus.com/wp-content/uploads/2021/10/4-Thomas-Fontaine_Hydrogen-project-in-Dijon_October-14-2021-1.pdf, accessed: 2024-09-30 (2021).
[32] L. Meillaud, Dijon ouvre sa première station d'hydrogène, https://hydrogentoday.info/dijon-premiere-station-hydrogene/, accessed: 2024-09-30 (2024).
[33] K. S. Anderson, C. W. Hansen, W. F. Holmgren, A. R. Jensen, M. A. Mikofski, A. Driesse, et al., pvlib python: 2023 project update, Journal of Open Source Software 8 (92) (2023) 5994.
[34] G. G. Electric, https://www.wind-turbine-models.com/manufacturers/26-ge-general-electric (2022).
[35] Danish Energy Agency, Technology Data, https://ens.dk/en/our-services/projections-and-models/technology-data (2023).
[36] A. X. Y. Mah, W. S. Ho, M. H. Hassim, H. Hashim, G. H. T. Ling, C. S. Ho, Z. Ab Muis, Optimization of a standalone photovoltaic-based microgrid with electrical and hydrogen loads, Energy 235 (2021) 121218.
[37] European Environment Agency, Greenhouse gas emission intensity of gdp, https://www.eea.europa.eu/en/analysis/indicators/greenhouse-gas-emission-intensity-of-1?activeAccordion=ecdb3bcf-bbe9-4978-b5cf-0b136399d9f8 (2024).
[38] B. Thomas, G. de Temmerman, R. Girard, J. Lamarque-Lacoste, M. d. l. M. Saint Pierre, A. Dubois, Low-carbon hydrogen production in the eu: are 2030 targets achievable? (2023).
[39] European Union, Regulation (eu) 2021/2139, https://eur-lex.europa.eu/legal-content/FR/TXT/HTML/?uri=CELEX:32021R2139&from=EN#d1e40-1-1 (2024).
[40] le gestionnaire du réseau de transport d'électricité français, https://www.rte-france.com/, accessed: May 5, 2023 (2023).
[41] M. Sengupta, Y. Xie, A. Lopez, A. Habte, G. Maclaurin, J. Shelby, The national solar radiation data base (nsrdb), Renewable and sustainable energy reviews 89 (2018) 51–60.
[42] M. M. Rienecker, M. J. Suarez, R. Gelaro, R. Todling, J. Bacmeister, E. Liu, M. G. Bosilovich, S. D. Schubert, L. Takacs, G. K. Kim, et al., Merra: Nasa's modern-era retrospective analysis for research and applications, J Clim 24 (14) (2011) 3624–3648.
[43] S. Haas, B. Schachler, U. Krien, S. Bosch, Windpowerlib-a python library to model wind power plants, 2019, Oemof Developer Group: Flensburg, Germany (2019).
[44] O. D. R. Énergies (ODRÉ), https://opendata.reseaux-energies.fr/" (2023).
[45] S. Basnet, KLMS-OPT, https://github.com/Bernhertz/H2-HRES-Scheduling (2025).
[46] M. L. Bynum, G. A. Hackebeil, W. E. Hart, C. D. Laird, B. L. Nicholson, J. D. Siirola, J.-P. Watson, D. L. Woodruff, et al., Pyomo-optimization modeling in python, Vol. 67, Springer, 2021.
[47] S. Basnet, K. Deschinkel, L. Le Moyne, M. C. Péra, Optimal integration of hybrid renewable energy systems for decarbonized urban electrification and hydrogen mobility, International Journal of Hydrogen Energy 83 (2024) 1448–1462.
[48] V. Badescu, A new kind of cloudy sky model to compute instantaneous values of diffuse and global solar irradiance, Theoretical and Applied Climatology 72 (2002) 127–136.
[49] S. Diaf, G. Notton, M. Belhamel, M. Haddadi, A. Louche, Design and techno-economical optimization for hybrid pv/wind system under various meteorological conditions, Applied energy 85 (10) (2008) 968–987.
[50] H. Tebibel, Methodology for multi-objective optimization of wind turbine/battery/electrolyzer system for decentralized clean hydrogen production using an adapted power management strategy for low wind speed conditions, Energy Conversion and Management 238 (2021) 114125.
[51] S. A. N'guessan, K. S. Agbli, S. Fofana, D. Hissel, Optimal sizing of a wind, fuel cell, electrolyzer, battery and supercapacitor system for off-grid applications, International Journal of Hydrogen Energy 45 (8) (2020) 5512–5525.
[52] K. Knosala, L. Kotzur, F. T. Röben, P. Stenzel, L. Blum, M. Robinius, D. Stolten, Hybrid hydrogen home storage for decentralized energy autonomy, international journal of hydrogen energy 46 (42) (2021) 21748–21763.
[53] B. Dursun, Determination of the optimum hybrid renewable power generating systems for kavakli campus of kirklareli university, turkey, Renewable and Sustainable Energy Reviews 16 (8) (2012) 6183–6190.
[54] S. Basnet, K. Deschinkel, L. Le Moyne, M. C. Péra, Optimizing grid-integrated renewable systems for cost-effective electricity and hydrogen supply, in: 2024 IEEE International Conference on Industrial Technology (ICIT), IEEE, 2024, pp. 1–8.
[55] Arrete, Arrêté du 1er juillet 2024 précisant le seuil d'émissions de gaz à effet de serre et la méthodologie pour qualifier l'hydrogène comme renouvelable ou bas-carbone (2024).
URL https://www.legifrance.gouv.fr/jorf/id/JORFTEXT000049870616
[56] S. Pookpunt, W. Ongsakul, Optimal placement of wind turbines within wind farm using binary particle swarm optimization with time-varying acceleration coefficients, Renewable energy 55 (2013) 266–276.
[57] C. Population, Dijon (dijon, côte-d'or, france) - population statistics, charts, map, location, weather and web information, https://www.citypopulation.de/en/france/cotedor/dijon/21231__dijon/ (2024).
[58] S. Basnet, Simulation of a hydrogen ecosystem, Ph.D. thesis, Université Marie et Louis Pasteur (2025).
[59] I. IRENA, Making the breakthrough: Green hydrogen policies and technology costs, Abu Dhabi: International Renewable Energy Agency (2021).